The Astrophysical Journal, 601:1075–1087, 2004 February 1


# COOL WHITE DWARFS REVISITED: NEW SPECTROSCOPY AND PHOTOMETRY

Samir Salim,[1,2] R. Michael Rich,[1,2] Brad M. Hansen,[1] L. V. E. Koopmans,[3] Ben R. Oppenheimer,[4] and Roger D. Blandford[5]

*Received 2003 August 7; accepted 2003 October 7*


## ABSTRACT

In this paper we present new and improved data on 38 cool white dwarfs identified in 2001 by Oppenheimer and coworkers as candidate dark-halo objects. Using the high-resolution spectra obtained with LRIS on Keck I, we measure precise radial velocities for 13 white dwarfs that show an H$\alpha$ absorption line. We show that accounting for radial velocities on average decreases the *U-V* plane velocities by only 6%. In two cases, accounting for the radial velocities put original halo candidates below the Oppenheimer and coworkers velocity cut. The radial velocity sample has a velocity dispersion in the direction perpendicular to the Galactic plane of $\sigma_W = 59$ km s$^{-1}$, between the values typically associated with the thick-disk and stellar-halo populations. We also see indications of the presence of two populations by analyzing the velocities in the *U-V* plane. In addition, we present CCD photometry for half of the sample, and with it recalibrate the photographic photometry of the remaining white dwarfs. Using the new photometry in standard bands and applying the appropriate color-magnitude relations for hydrogen and helium atmospheres, we obtain new distance estimates. By recalibrating the distances of the white dwarfs that were not originally selected as halo candidates, we obtain 13 new candidates (and lose two original ones). On average, the new distances produce velocities in the *U-V* plane that are larger by 10%, with already fast objects gaining more. Using the new data while applying the same *U-V* plane velocity cut (94 km s$^{-1}$) and methods of analysis as did Oppenheimer and coworkers, we find a density of cool white dwarfs of $1.7 \times 10^{-4}$ pc$^{-3}$, confirming their value. In addition, we derive the density as a function of the *U-V* plane velocity cutoff. The density (corrected for losses due to higher *U-V* plane velocity cuts) starts to flatten out at 150 km s$^{-1}$ ($0.4 \times 10^{-4}$ pc$^{-3}$) and is minimized (thus minimizing the possible nonhalo contamination) at 190 km s$^{-1}$ ($0.3 \times 10^{-4}$ pc$^{-3}$). These densities are in rough agreement with the estimates for the *stellar-halo* white dwarfs, corresponding to values a factor of 1.9 and 1.4 higher.


*Subject headings:* dark matter — Galaxy: halo — stars: kinematics — white dwarfs

## 1. INTRODUCTION

Dynamical studies indicate that large quantities of gravitating matter exist in the halos of galaxies, including our own. The amount of this matter far surpasses that of matter with detectable electromagnetic radiation. Revealing the nature of this so called "dark matter" is one of the crucial goals in present-day astronomy and cosmology.

One of the first proposed methods of indirectly detecting dark matter was to look for lensing of background stars by dark objects in the Galactic halo (Paczyński 1986). This technique, microlensing, is sensitive to macroscopic objects, known as MACHOs, ranging in mass from planetary to stellar. At the time when the first microlensing experiments began, there was still no consensus as to whether dark matter halos were baryonic or nonbaryonic. With the exception of primordial black holes, microlensing exclusively detects baryonic matter. Now, after years of observing, microlensing has ruled out a dark halo made entirely of MACHOs but has nonetheless found more lensing events than expected from the known stellar populations, either in the Galactic disk and halo or in the LMC (or SMC), where the lensed stars reside. The latest estimate from the MACHO group favors a halo in which dark objects comprise 20%, each with a typical mass of 0.6 $M_\odot$ (Alcock et al. 2000). Another microlensing experiment, EROS, finds upper limits for stellar-mass compact halo objects of 30% from monitoring the LMC (Lasserre et al. 2000) and 25% from the SMC (Afonso et al. 2003). Some researchers (e.g., Sahu 1994) believe that the lenses responsible for these events reside in the LMC (or SMC) itself; however, these scenarios have their own problems.

Since the search for dark matter in the form of MACHOs began, our paradigms about what cosmological dark matter should be have changed. With the discovery of cosmological acceleration due to "dark energy" (Garnavich et al. 1998; Riess et al. 1998), the discrepancy between the critical mass density required by the inflationary model and the low observed densities of gravitating matter was reconciled. Cosmological models preferred genuine dark matter to be in the form of *nonbaryonic* cold dark matter, concentrated in galactic halos. In addition to that, a large fraction, or all, of the *baryonic* matter that was previously unaccounted for is now believed to reside in systems such as those responsible for the population of Ly$\alpha$ absorbers.

This alone would be enough to shift the focus of observations to the detection of nonbaryonic halo dark matter (in the form of particles) were it not for the MACHO results suggesting unknown dark objects. Making the problem more severe, there are a number of theoretical and observational arguments suggesting that baryonic matter should at most constitute only a negligible fraction of a dark halo, much lower than the fraction of it believed to be in MACHOs (Freese, Fields, & Graff 2000). Of

[1] Department of Physics and Astronomy, University of California at Los Angeles, Los Angeles, CA 90095; samir@astro.ucla.edu, rmr@astro.ucla.edu, hansen@astro.ucla.edu.

[2] Visiting Astronomer, Lick Observatory.

[3] Space Telescope Science Institute, Baltimore, MD 21218; koopmans@stsci.edu.

[4] Astrophysics Department, American Museum of Natural History, New York, NY 10024; bro@amnh.org.

[5] Theoretical Astrophysics, California Institute of Technology, Pasadena, CA 91125; rdb@tapir.caltech.edu.

the various candidate counterparts to MACHOs, ancient, cool white dwarfs (WDs) are the best, especially since their expected masses are comparable. The main questions, then, are whether we can detect these halo WDs and, if so, what fraction of the dark-halo mass they constitute. Ideally, these WDs should account for *all* MACHOs; otherwise, yet another form of baryonic dark matter is required.

Surveying 10% of the sky and using a proper motion–selected sample of objects with high reduced proper motions, Oppenheimer et al. (2001, hereafter OHDHS) have identified and spectroscopically confirmed 98 WDs, 38 of which have halo-like kinematics based on their derived velocity components in the plane of the Galaxy (*U*-*V* plane). The derived mass density of these cool WDs indicates that they make up at least $\sim$2% of the local dark matter halo density, an order of magnitude higher than expected from the population of stellar-halo (as opposed to dark-halo) WDs. Stellar-halo WDs should differ from the dark-halo ones in their origin, since the dark-halo WDs were presumably produced in an early burst of star formation and have been cooling ever since. The OHDHS paper and its results stirred the astronomical community, generating numerous objections regarding the selection of objects, kinematical cuts, contamination from nonhalo populations, and so on. A thorough review on the subject of cool WDs and of various interpretations of the OHDHS work is given by Hansen & Liebert (2003).

In this paper we reanalyze the OHDHS sample of cool WDs using newly acquired high-resolution spectra and CCD imaging. The new data allow measurement of radial velocities and determination of photometric distances in a more direct and precise manner, thus addressing some issues raised with respect to the original OHDHS data. (OHDHS used classification-grade, low-resolution spectra and photometry derived from photographic plates.)

In § 2 we present spectroscopic observations and the derivation of radial velocities for WDs exhibiting spectral features. Photometry from the CCD imaging is presented in § 3, together with a calibration of the photographic magnitudes used by OHDHS. In § 4 we assemble all data to produce a new data set, required for kinematical analysis. Finally, in § 5 we discuss the properties of the revised kinematical data set and use them to address some of the issues raised against the original OHDHS sample and its interpretation. In particular, we recalculate the densities of WDs using the OHDHS velocity cut but also as a function of the cutoff velocity. In a forthcoming work, the new data set will be analyzed with additional techniques, including the kinematical modeling of stellar populations.

## 2. SPECTROSCOPY

### 2.1. *Observations and Data Reduction*

The spectra of OHDHS cool WDs were taken with the LRIS (Oke et al. 1995) spectrograph on Keck I, on three nights: 2002 September 13 and 14 and 2002 December 4 (UT). The primary goal was to obtain high-resolution spectra in the region around the H$\alpha$ $\lambda$6563 line. Thus, the spectroscopic setup in the red arm of LRIS consisted of the 1200/7500 grating, giving a dispersion of 0.63 Å pixel$^{-1}$ and a spectral coverage of 5850–7140 Å. The only exceptions to this setup were in the cases of WDs with peculiar spectra (that happened to show no hydrogen lines): WD 2356−209[6] and LHS 1402. The first was imaged in both the high-resolution and low-resolution modes, while the second was only in the low-resolution mode: 300/5000 grating, 2.46 Å pixel$^{-1}$ dispersion, and 5010–10030 Å range. The slit width of 1″ gave an effective resolution in the high-resolution mode of 2.9 Å. On 2002 December 4, one additional WD was observed (WD 2346−478), this time with the 831/8200 grating (0.92 Å pixel$^{-1}$ dispersion, 5630–7500 Å range).

The cumulative exposure times varied from 6 to 45 minutes. Calibration lamp spectra were obtained at each pointing, and internal-lamp flat-field images were taken once a night. Standard extraction and calibration IRAF tasks were employed to produce the final spectra.

### 2.2. *Measuring Radial Velocities*

Measuring the radial velocities was the main goal of the high-resolution spectroscopy observing program. Targets were selected by inspecting the low-resolution spectra obtained by OHDHS. They found an H$\alpha$ line in 14 out of 38 cool WDs (denoted with an asterisk in OHDHS Table 1). Of these 14, all but three can be observed from Keck's latitude, and we have obtained spectra of all 11. In addition, we took spectra of another 12 WDs thought to be featureless. Among these we find an additional two with an H$\alpha$ line. Thus, our radial velocity sample comprises 13 cool WDs.

The wavelength region covered by the high-resolution spectra would allow detection of lines other than that of hydrogen (such as He and C). However, careful inspection of the spectra (with signal-to-noise ratios [S/Ns] ranging from $\sim$30 to $\sim$110) does not reveal any such lines.

Each individual spectrum was wavelength-calibrated against a lamp spectrum. The typical rms of the calibration was 0.02 Å. The wavelengths of the lines were first measured in individual spectra (of the same object) in order to evaluate the stability of the zero point of the wavelength calibration and to establish the accuracy with which the central wavelength of H$\alpha$ could be determined. All measurements were done using the *splot* routine in IRAF. WD spectra were normalized by the continuum, and a Lorentzian function was used to fit the lines.

The stability of the zero point of the calibration was determined by measuring a bright sky emission line of [O I] at 6300.304 Å. The measured mean wavelength was 6300.30 $\pm$ 0.01 Å, indicating no systematic shifts in the calibration, while the scatter around the mean of 0.07 Å (equivalent to 3 km s$^{-1}$) gives the level of radial velocity error due to the wavelength calibration.

The spectra of WDs have different levels of S/N, leading to variations in the quality of the H$\alpha$ profile. In well-exposed spectra, the non-LTE core of the H$\alpha$ line is well defined, so measuring the central wavelength of the core would be superior to fitting a profile to the entire line. However, in lower S/N spectra, the core may be degraded by noise. In order to test which method was more appropriate for our sample, we compared line fitting to the *entire* profile (6400–6800 Å; which fitted the wing portions of the profile well but often failed to fit the core) with the fitting of the non-LTE core alone (width $\sim$5 Å). For each method, we first found the difference of the individual measurements with respect to the mean value (for a given object) and then calculated the overall scatter. For wide-profile fitting the scatter was 0.45 Å, while for core fitting it was 0.32 Å. In other words, core fitting seems to have better repeatability and should thus be more precise. We should also note that we do not observe cases of split cores or emission in the cores.

[6] We use the same WD designations as in OHDHS.

Since the scatter, i.e., the error of the individual measurements, was much larger than the stability of the zero point of the wavelength calibration, we concluded that it was safe to *combine* the spectra belonging to the same object (between three and six), thus obtaining a higher signal and eliminating deviant points by performing $\sigma$-clipping. Since the spectra of a given object were taken over a short period of time, the heliocentric velocity correction need not have been applied at this stage. We then proceeded by finding the central wavelengths of the H$\alpha$ lines in the combined spectra, again by fitting a Lorentzian to the core. This gave our final measured wavelength. In order to evaluate the measurement error, we evaluated, as a function of the measured flux, the rms scatter of the central wavelengths of individual spectra belonging to a given object. Not surprisingly, the scatter is larger for objects whose individual spectra have low intensities. We find a linear relation between the logarithm of flux and the rms scatter of individual wavelength measurements. However, at a certain flux level, the rms reaches a minimum value of 0.13 Å, despite the increase of signal. In the fluxes of the *combined* spectra, this plateau is actually reached for most spectra in our sample. Thus, for most spectra, the total error from noise and wavelength calibration uncertainties is equivalent to $\approx$7 km s$^{-1}$, well within the limits acceptable for this study. Finally, to get the measured radial velocity, we apply the heliocentric correction. The observed radial velocities of 13 WDs and their errors are listed in Table 1. Also listed are 10 WDs observed with LRIS but lacking spectral features.

## 3. PHOTOMETRY

### 3.1. *Observations and Data Reduction*

Photometry was performed on CCD images taken with the 1 m Nickel Telescope at the Lick Observatory, on 2002 November 27 and December 3 and 4 (UT). The Dewar 2 CCD, with a high quantum efficiency extending to blue wavelengths, was used. The first two nights were fully photometric, and many standards over a large range of air masses and colors were observed. This allowed construction of photometric transformations with linear and quadratic color terms. The photometric accuracy from calibration was 0.01–0.02 mag in all bands.

TABLE 1
OBSERVED WDs AND THEIR RADIAL VELOCITIES

| Number[a] | Name | $v_{\rm rad}^{\rm obs}$ (km s$^{-1}$) |
|---|---|---|
| 2..... | WD 0153−014 | −50 ± 7 |
| 5..... | LHS 147 | −15 ± 7 |
| 7..... | WD 0135−039 | −28 ± 7 |
| 8..... | LHS 4042 | −24 ± 7 |
| 9..... | WD 2356−209 | ... |
| 10..... | WD 0227−444 | ... |
| 12..... | LHS 4033 | 206 ± 7 |
| 13..... | LP 586-51 | −22 ± 7 |
| 14..... | WD 2242−197 | −8 ± 7 |
| 15..... | WD 0205−053 | ... |
| 17..... | WD 0125−043 | ... |
| 18..... | WD 2346−478 | 75 ± 7 |
| 20..... | WD 0300−044 | 141 ± 13 |
| 21..... | WD 0123−278 | ... |
| 24..... | LHS 1402 | ... |
| 25..... | LHS 1274 | 81 ± 7 |
| 27..... | WD 0044−284 | ... |
| 28..... | WD 2214−390 | 50 ± 7 |
| 30..... | LP 588-37 | −127 ± 7 |
| 32..... | WD 0045−061 | ... |
| 33..... | WD 0225−326 | ... |
| 35..... | WD 0117−268 | ... |
| 36..... | LP 651-74 | 74 ± 7 |

NOTE.—In cases in which no features were detected, radial velocity was omitted.
[a] The numbering follows Table 1 of OHDHS.

Of the 38 cool WDs, 19 reach an altitude high enough to be observed with this telescope. Of these, 18 were imaged in the *V* and *I* (Cousins) bands. In addition, nine of those were also observed in the *B* band, and a further three in the *R* band. Of the 18 WDs with *VI* photometry, nine also belong to the radial velocity sample.

Object photometry was performed with an aperture equal to 1 FWHM of the point-spread function (typically 2.″4) and then aperture-corrected using a bright, isolated star in the field. All *I*-band images were corrected for fringing. For each measurement, the photon error from the object was combined with the photon error from the aperture correction star. The individual measurements were transformed into standard magnitudes and combined (weighted by photometric errors) into a single magnitude per star per band. The median photometry errors of the WD sample are $\langle\sigma_B\rangle = 0.053$, $\langle\sigma_V\rangle = 0.035$, $\langle\sigma_R\rangle = 0.030$, and $\langle\sigma_I\rangle = 0.035$. The median error of $V-I$ color, which we use to deduce distances, is 0.052 mag. The photometry is summarized in Table 2.

Since most of the cool WDs were not known before, it is not surprising that the literature search for photometric data produced prior measurements for only two WDs: LHS 542 and LHS 147. The comparison of their photometry with ours is given in Table 3. They are in excellent agreement. Photometric magnitudes in other bands do exist for several WDs in Sloan Digital Sky Survey (SDSS) Data Release 1 and for nine WDs in the 2MASS (Two Micron All Sky Survey) All-Sky Point Source Catalog. The 2MASS measurements are discussed in § 4.3.1.

### 3.2. *Photometric Calibration of OHDHS Magnitudes*

Since we obtained CCD photometry for only one-half of the OHDHS sample, it would be useful to derive photometry of other objects in standard bands. Thus, we would like to construct empirical transformations between the photographic plate magnitudes used by OHDHS, $B_{\rm J}$, $R_{59\rm F}$, and $I_{\rm N}$, and the standard photometric bands. Empirical transformations between photographic and standard magnitudes do exist in the literature, while synthetic transformations can be constructed using model spectra and transmission curves, yet the first method has not been specifically applied to stars such as cool WDs, while the second suffers from often ill-defined properties of the actual response of a given plate/filter combination.

Here we derive relations between photographic and standard magnitudes as measured by CCD photometry. For $B_{\rm J}$,

$$B_{\rm J} = B - 0.85(B - V) + 0.26. \quad (1)$$

This relation has $\sigma = 0.10$. Since we know that $\sigma_B = 0.05$, this indicates that $\sigma_{B_{\rm J}} = 0.08$, which is quite remarkable for photographic photometry. Note that a high color term indicates that (at least for WDs) $B_{\rm J}$ is actually closer to standard *V* than to standard *B*.

For $R_{59\rm F}$,

$$R_{59\rm F} = V - 0.66(V - I) + 0.13. \quad (2)$$

TABLE 2
JOHNSON-COUSINS CCD PHOTOMETRY

| Number[a] | Name | $B$ | $V$ | $R$ | $I$ | $n_{obs}$[b] |
|---|---|---|---|---|---|---|
| 2 | WD 0153−014 | ... | 18.646 ± 0.020 | ... | 18.415 ± 0.034 | 0202 |
| 3 | LHS 542 | 19.473 ± 0.053 | 18.221 ± 0.023 | 17.545 ± 0.025 | 16.926 ± 0.028 | 2321 |
| 5 | LHS 147 | 17.985 ± 0.018 | 17.615 ± 0.011 | ... | 17.169 ± 0.016 | 3202 |
| 6 | WD 2326−272 | 21.027 ± 0.165 | 19.922 ± 0.051 | ... | 19.095 ± 0.051 | 2202 |
| 7 | WD 0135−039 | ... | 19.644 ± 0.048 | ... | 19.083 ± 0.065 | 0402 |
| 9 | WD 2356−209 | 21.206 ± 0.109 | 20.850 ± 0.075 | ... | 18.878 ± 0.033 | 2404 |
| 12 | LHS 4033 | 17.162 ± 0.020 | 16.992 ± 0.017 | 16.987 ± 0.030 | 16.936 ± 0.036 | 3222 |
| 13 | LP 586-51 | 18.318 ± 0.039 | 18.185 ± 0.022 | 18.141 ± 0.044 | 18.096 ± 0.039 | 1212 |
| 14 | WD 2242−197 | 20.504 ± 0.098 | 19.659 ± 0.045 | ... | 18.861 ± 0.074 | 1201 |
| 15 | WD 0205−053 | ... | 18.898 ± 0.145 | ... | 17.257 ± 0.024 | 0101 |
| 17 | WD 0125−043 | ... | 19.820 ± 0.076 | ... | 18.911 ± 0.054 | 0202 |
| 20 | WD 0300−044 | 20.782 ± 0.266 | 19.862 ± 0.049 | ... | 19.301 ± 0.051 | 1404 |
| 24 | LHS 1402 | ... | 18.050 ± 0.014 | ... | 18.422 ± 0.027 | 0205 |
| 27 | WD 0044−284 | ... | 20.022 ± 0.060 | ... | 18.713 ± 0.039 | 0402 |
| 30 | LP 588-37 | ... | 18.496 ± 0.024 | ... | 18.365 ± 0.039 | 0303 |
| 32 | WD 0045−061 | ... | 18.203 ± 0.015 | ... | 17.219 ± 0.019 | 0302 |
| 35 | WD 0117−268 | ... | 19.057 ± 0.049 | ... | 17.944 ± 0.030 | 0303 |
| 36 | LP 651-74 | 18.033 ± 0.021 | 17.342 ± 0.011 | ... | 16.568 ± 0.015 | 2202 |

[a] The numbering follows Table 1 of OHDHS.
[b] Number of observations for each band: *BVRI*.

Since we have our $R$ for only three objects, we give this transformation relative to $V$. Excluded from the fit is LHS 1402, a peculiar WD. The derived accuracy of the relation is 0.10 mag, while $\sigma_{R_{59F}} = 0.09$.

For $I_N$,

$$I_N = I - 0.09(V - I) + 0.12. \quad (3)$$

This relation has $\sigma \approx \sigma_{I_N} = 0.16$. Excluding objects for which OHDHS derive $I_N$ spectrophotometrically does not change the above relation.

Another source of photographic magnitudes is the recently completed USNO-B catalog (a similar catalog, Guide Star Catalog 22, does not go deep enough in most cases). We have matched all the objects to counterparts in the USNO-B catalog (Monet et al. 2003) and have repeated the above analysis against $B_2$, $R_2$, and $I_{SERC}$—second-generation sky survey magnitudes from USNO-B. However, we find that USNO-B magnitudes are significantly inferior to those used by OHDHS, despite the fact that they come from similar or the same plate material. Namely, we find $\sigma_{B_2} = 0.41$, $\sigma_{R_2} = 0.58$, and $\sigma_{I_{SERC}} = 0.26$.

Overall, we conclude that the OHDHS photographic plate photometry (that is, the SuperCOSMOS Sky Survey from which it is taken; Hambly, Irwin, & MacGillivray 2001b; Hambly et al. 2001a) is of excellent quality, which lends credence to transforming the photographic magnitudes into standard magnitudes in order to derive photometric distances.

Since we are obtaining distances from the $V$ magnitude and $V-I$ color, we want to directly transform OHDHS magnitudes and colors to these. We have seen that $B_J$ is quite close to $V$, so we use that magnitude to obtain the transformations

$$V = B_J - 0.23(B_J - I_N) - 0.17, \quad \sigma = 0.12, \quad (4)$$

$$V - I = 0.62(B_J - I_N) - 0.04, \quad \sigma = 0.08. \quad (5)$$

These calibrations were derived omitting both peculiar-spectra WDs (LHS 1402 and WD 2356−209).

## 4. THE NEW DATA SET

### 4.1. *Radial Velocities*

#### 4.1.1. *Gravitational Redshifts*

The observed radial velocities (Table 1) were extracted as explained in § 2. However, they do not represent the true radial velocities, since WDs exhibit substantial gravitational redshift. The exact redshift depends on the mass and the radius of a WD, which we do not know for individual WDs in our sample. However, it is known that the range of these values is

TABLE 3
COMPARISON WITH THE PUBLISHED PHOTOMETRY

| Name | $B$ | $V$ | $R$ | $I$ | Reference |
|---|---|---|---|---|---|
| LHS 542 | 19.23 | 18.15 | 17.53 | 16.99 | 1 |
| | 19.49 | 18.25 | ... | ... | 2 |
| | 19.47 | 18.22 | 17.55 | 16.93 | 3 |
| LHS 147 | 17.97 | 17.62 | 17.38 | 17.16 | 4 |
| | 18.09 | 17.66 | ... | ... | 2 |
| | 17.94 | 17.57 | ... | ... | 5 |
| | 17.99 | 17.62 | ... | 17.17 | 3 |

REFERENCES.—(1) Bergeron et al. 2001; (2) Liebert, Dahn, & Monet 1988; (3) this work; (4) Bergeron et al. 1997; (5) Eggen & Sandage 1967.

relatively small, so for our purposes it is sufficient to adopt a common value for the redshift. From Reid (1996) we find that field WDs have an average redshift of 28.6 km $s^{-1}$, with a spread of 6.5 km $s^{-1}$. We subtract this value from the observed radial velocities and add the scatter to the radial velocity measurement error. The final values are listed in Table 4.

#### 4.1.2. *Common Proper-Motion Binaries*

In the case in which a WD has a common proper-motion companion that is a main-sequence star, one can obtain a measurement of the true radial velocity of the WD (whether it contains spectral lines or not) simply by measuring the radial velocity of the main-sequence component. Such a measurement circumvents the gravitational redshift correction. To this end, we have carried out a search for companions in the USNO-B catalog, which lists proper motions based on multiple plates. Within the 2′ search radius, we find no candidate companions with proper motions compatible with those of the WDs.

#### 4.1.3. *Selection Effects*

The original OHDHS selection of cool WDs was based on the $U$- and $V$-components of the velocity. In the absence of radial velocities, they were calculated by assuming $W = 0$. Since our goal is to characterize this population by obtaining the third component of the velocity from the radial velocities, we should try to evaluate whether the subsample for which radial velocities are measured is representative of the population as a whole. Here we restrict ourselves to the question of whether the subsample is representative *kinematically*, in terms of its $U$- and $V$-velocities, based on which cool WD sample was selected in the first place.

OHDHS selected their sample by requiring the WDs to have a velocity above some threshold in the $U$-$V$ plane. This threshold was chosen as the 2 $\sigma$ $U$-$V$ plane velocity of the thick-disk population:

$$U\text{-}V \equiv \sqrt{U^2 + (V + 35 \text{ km s}^{-1})^2} > 94 \text{ km s}^{-1}. \quad (6)$$

One way of characterizing whether the subsample of 13 WDs with radial velocities is representative is to compare its average $U$-$V$ plane velocity with the typical $U$-$V$ plane velocities of randomly selected subsamples of 13 WDs out of the total 38.

In order to obtain the distribution of $U$-$V$ plane velocities of random subsamples, we run a Monte Carlo simulation that draws 13 out of 38 WDs numerous times and for each drawing calculates the average $U$-$V$ plane velocity. The average is taken in two ways: as a straight average and as a weighted average,

$$\langle U\text{-}V \rangle = \frac{\sum (U\text{-}V/\mathcal{V}_{\max})}{\sum (1/\mathcal{V}_{\max})},$$

where the weights are the corresponding maximum volumes in which a WD could have been detected in the OHDHS survey. As explained in OHDHS, for each individual object, $\mathcal{V}_{\max}$ is set by either the magnitude limit of the survey or the lower proper-motion cutoff, whichever is smaller. In Figure 1 the solid line represents the distribution of unweighted averages. The unweighted average of the radial velocity sample is 195 km $s^{-1}$ and is indicated by the arrow. We see that it is on the high side of the distribution (thus, somewhat favoring fast objects) but well within the spread of the distribution. The weighted $U$-$V$ plane velocity distribution (*dashed line*) has two peaks, the lower being dominated by proper motion–limited objects and the higher by the magnitude-limited ones. That we see two peaks might actually be indicative of the fact that the OHDHS sample is composed of more than one population. We see that the weighted average of our radial velocity sample lies right at the proper motion–limited peak. If there really are two different populations, this might mean that our radial velocity subsample is primarily representative of one of these populations, the one with intrinsically lower velocities. This is further discussed in § 5.3. In any case, the radial velocity subsample does not seem to be extreme with respect to the whole sample in terms of its $U$-$V$ plane kinematics.

### 4.2. *Proper Motions*

Proper motions enter into the kinematical data set since, together with the distance, they determine two components of the physical velocity. OHDHS proper motions come from the SuperCOSMOS Sky Survey (Hambly et al. 2001c). Since the OHDHS sample consists of relatively high proper motion stars, the average fractional error is small (7% from listed values) and is thus not going to dominate in the velocity error, especially since the distances were originally derived from plate photometry. Although not as important as other recalibrations, we nevertheless carry out a comparison of SuperCOSMOS proper motions of OHDHS WDs with those from the USNO-B catalog. USNO-B combines a large number of plates to arrive at a proper-motion solution, the errors of which are found to be reliable (Gould 2003). In this comparison we use data from B. Oppenheimer's on-line table,[7] since unlike

[7] Available at http://research.amnh.org/users/bro and the VizieR catalog service at CDS.

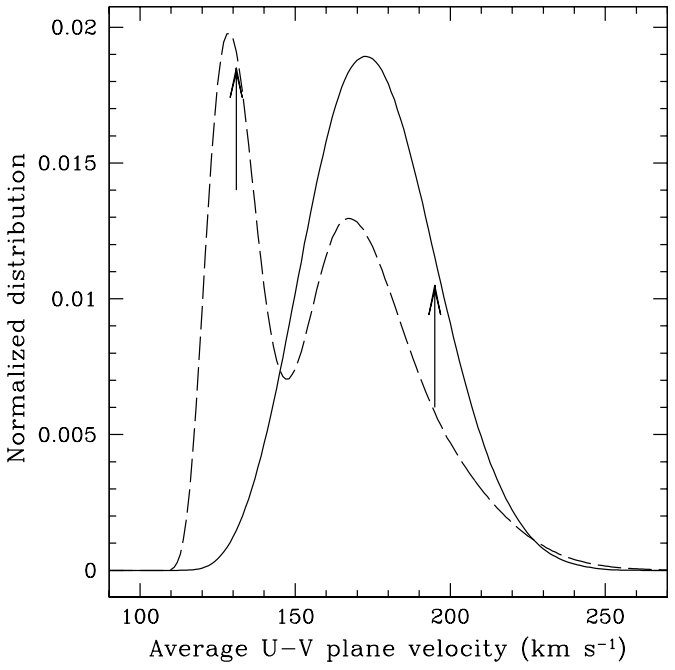


FIG. 1.—Kinematical selection effects of the radial velocity subsample. The two curves show the straight (*solid line*) and weighted (*dashed line*) average $U$-$V$ plane velocity ($U\text{-}V \equiv [U^2 + (V + 35 \text{ km s}^{-1})^2]^{1/2}$) of random subsamples of 13 WDs (out of 38 OHDHS cool WDs). Compared with these distributions are the actual (straight and weighted) $U$-$V$ plane velocity averages of our radial velocity subsample, shown with arrows.

TABLE 4

THE NEW DATA SET: RELEVANT DATA ON COOL WHITE DWARFS

| Number | Name | R.A. (deg) | Decl. (deg) | $\mu_\alpha$ (mas yr$^{-1}$) | $\mu_\delta$ (mas yr$^{-1}$) | $\sigma(\mu_\alpha)$ (mas yr$^{-1}$) | $\sigma(\mu_\delta)$ (mas yr$^{-1}$) | Flag A[a] | $V$ (mag) | $V-I$ (mag) | Flag P[b] | $d$ (pc) | $\sigma$ ($d$) (pc) | Flag C[c] | $v_{\rm rad}$ (km s$^{-1}$) | $\sigma(v_{\rm rad})$ (km s$^{-1}$) |
|---|---|---|---|---|---|---|---|---|---|---|---|---|---|---|---|---|
| 1..... | F351-50 | 11.33178 | −33.49130 | 1860 | −1486 | 51 | 10 | U | 19.37 | 1.54 | O | 40 | 10 | He | ... | ... |
| 2..... | WD 0153−014 | 28.46448 | −1.39468 | 64 | −398 | 4 | 6 | U | 18.65 | 0.23 | S | 170 | 36 | H | −79 | 9 |
| 3..... | LHS 542 | 349.78956 | −6.21383 | −618 | −1584 | 1 | 5 | U | 18.22 | 1.29 | S | 31 | 7 | He | ... | ... |
| 4..... | WD 0351−564 | 57.78907 | −56.45198 | 265 | −1052 | 20 | 19 | O | 20.96 | 1.49 | O | 88 | 22 | He | ... | ... |
| 5..... | LHS 147 | 27.03805 | −17.20401 | −120 | −1106 | 7 | 6 | U | 17.61 | 0.45 | S | 75 | 15 | H | −44 | 9 |
| 6..... | WD 2326−272 | 351.54458 | −27.24632 | 576 | −104 | 4 | 9 | U | 19.92 | 0.83 | S | 112 | 27 | He | ... | ... |
| 7..... | WD 0135−039 | 23.89029 | −3.95502 | 454 | −186 | 7 | 6 | U | 19.64 | 0.56 | S | 160 | 38 | H | −57 | 9 |
| 8..... | LHS 4042 | 358.64586 | −32.35540 | 422 | −46 | 1 | 10 | U | 17.41 | 0.18 | O | 105 | 25 | H | −52 | 9 |
| 9..... | WD 2356−209 | 359.18788 | −20.91370 | −329 | −211 | 32 | 20 | O | 20.85 | 1.97 | S | 74 | 34 | Sp | ... | ... |
| 10..... | WD 0227−444 | 36.87318 | −44.38573 | 268 | −217 | 12 | 18 | O | 19.82 | 1.06 | O | 83 | 22 | He? | ... | ... |
| 11..... | J0014−3937 | 3.44777 | −39.62331 | −226 | −714 | 17 | 2 | U | 18.70 | 1.25 | O | 40 | 10 | He | ... | ... |
| 12..... | LHS 4033[d] | 358.13289 | −2.88647 | 614 | 324 | 10 | 8 | U | 16.99 | 0.06 | S | 105 | 22 | H | 178 | 9 |
| 13..... | LP 586-51 | 15.53001 | −0.54986 | 342 | −122 | 3 | 3 | U | 18.19 | 0.09 | S | 172 | 37 | H | −51 | 9 |
| 14..... | WD 2242−197 | 340.43428 | −19.67841 | 346 | 62 | 4 | 4 | U | 19.66 | 0.80 | S | 111 | 27 | H | −36 | 9 |
| 15..... | WD 0205−053 | 31.29830 | −5.29836 | 956 | 400 | 3 | 6 | U | 18.90 | 1.64 | S | 29 | 8 | He | ... | ... |
| 16..... | WD 0100−645 | 15.20987 | −64.48649 | 516 | 190 | 5 | 0 | U | 17.58 | 0.58 | O | 60 | 14 | H | ... | ... |
| 17..... | WD 0125−043 | 21.27431 | −4.28424 | 250 | −44 | 6 | 4 | U | 19.82 | 0.91 | S | 98 | 25 | He | ... | ... |
| 18..... | WD 2346−478 | 356.51213 | −47.85060 | −270 | −454 | 5 | 3 | U | 17.95 | 0.83 | O | 48 | 11 | H | 47 | 10 |
| 19..... | LHS 1447 | 42.05496 | −30.02575 | 436 | 322 | 0 | 6 | U | 18.43 | 0.44 | O | 106 | 25 | He | ... | ... |
| 20..... | WD 0300−044 | 45.09852 | −4.42355 | 272 | −280 | 17 | 19 | O | 19.86 | 0.56 | S | 177 | 41 | H | 112 | 15 |
| 21..... | WD 0123−278 | 20.76574 | −27.80398 | 342 | 124 | 5 | 16 | U | 20.29 | 1.29 | O | 80 | 26 | He? | ... | ... |
| 22..... | WD 2259−465 | 344.77772 | −46.46632 | 404 | −158 | 4 | 7 | U | 19.71 | 1.26 | O | 64 | 20 | He? | ... | ... |
| 23..... | WD 0340−330 | 55.03620 | −33.01671 | 494 | −330 | 3 | 5 | U | 19.94 | 1.17 | O | 77 | 22 | He? | ... | ... |
| 24..... | LHS 1402 | 36.13432 | −28.91646 | 492 | −30 | 3 | 2 | U | 18.05 | −0.37 | S | 21 | 5 | Sp | ... | ... |
| 25..... | LHS 1274 | 24.80995 | −33.81756 | 580 | −24 | 3 | 11 | U | 17.34 | 0.49 | O | 62 | 15 | H | 52 | 9 |
| 26..... | WD 0214−419 | 33.56203 | −41.85251 | 320 | −96 | 18 | 19 | O | 20.08 | 0.98 | O | 102 | 25 | He | ... | ... |
| 27..... | WD 0044−284 | 11.00892 | −28.40313 | −78 | −360 | 13 | 3 | U | 20.02 | 1.31 | S | 69 | 23 | He? | ... | ... |
| 28..... | WD 2214−390 | 333.64480 | −38.98522 | 1006 | −360 | 2 | 8 | U | 16.14 | 0.67 | O | 27 | 6 | H | 21 | 9 |
| 29..... | WD 2324−595 | 351.04227 | −59.46895 | 124 | −576 | 5 | 7 | U | 16.90 | 0.14 | O | 88 | 21 | H | ... | ... |
| 30..... | LP 588-37 | 25.58649 | −1.39757 | 108 | −344 | 1 | 7 | U | 18.50 | 0.13 | S | 186 | 40 | H | −155 | 9 |
| 31..... | WD 0345−362 | 56.38631 | −36.18446 | 142 | −588 | 18 | 67 | U | 20.40 | 1.45 | O | 71 | 17 | He | ... | ... |
| 32..... | WD 0045−061 | 11.27623 | −6.13876 | 104 | −676 | 3 | 3 | U | 18.20 | 0.98 | S | 43 | 10 | He | ... | ... |
| 33..... | WD 0225−326 | 36.36950 | −32.63163 | 310 | 160 | 36 | 4 | U | 18.61 | 0.40 | O | 118 | 28 | He | ... | ... |

TABLE 4—*Continued*

| Number | Name | R.A. (deg) | Decl. (deg) | $\mu_\alpha$ (mas yr$^{-1}$) | $\mu_\delta$ (mas yr$^{-1}$) | $\sigma(\mu_\alpha)$ (mas yr$^{-1}$) | $\sigma(\mu_\delta)$ (mas yr$^{-1}$) | Flag A[a] | $V$ (mag) | $V-I$ (mag) | Flag P[b] | $d$ (pc) | $\sigma$ ($d$) (pc) | Flag C[c] | $v_{\rm rad}$ (km s$^{-1}$) | $\sigma(v_{\rm rad})$ (km s$^{-1}$) |
|---|---|---|---|---|---|---|---|---|---|---|---|---|---|---|---|---|
| 34..... | WD 2348−548 | 357.19527 | −54.76280 | 364 | −96 | 22 | 32 | U | 19.21 | 0.98 | O | 69 | 17 | He | ... | ... |
| 35..... | WD 0117−268 | 19.46521 | −26.81428 | 476 | 42 | 3 | 3 | U | 19.06 | 1.11 | S | 55 | 15 | He? | ... | ... |
| 36..... | LP 651-74 | 46.80880 | −7.24976 | −193 | −436 | 11 | 10 | O | 17.34 | 0.77 | S | 40 | 8 | H | 45 | 9 |
| 37..... | WD 0135−546 | 23.91108 | −54.59108 | 660 | 108 | 17 | 3 | U | 18.91 | 1.13 | O | 51 | 14 | He? | ... | ... |
| 38..... | WD 0100−567 | 15.17948 | −56.77684 | 293 | 293 | 6 | 8 | O | 17.44 | 0.60 | O | 55 | 13 | H | ... | ... |
| A1..... | WD 2221−402 | 335.46833 | −40.19267 | 316 | −238 | 17 | 0 | U | 19.81 | 1.09 | O | 80 | 20 | He | ... | ... |
| A2..... | WD 2342−225 | 355.56890 | −22.45330 | 312 | 90 | 6 | 2 | U | 19.41 | 0.82 | O | 90 | 22 | He | ... | ... |
| A3..... | WD 0007−031 | 1.77802 | −3.11857 | 224 | −390 | 3 | 4 | U | 18.44 | 0.79 | O | 64 | 15 | H? | ... | ... |
| A4..... | WD 2236−168 | 339.06532 | −16.79833 | 318 | −60 | 3 | 6 | U | 18.48 | 0.75 | O | 69 | 17 | He | ... | ... |
| A5..... | WD 2234−408 | 338.72467 | −40.75506 | 287 | −249 | 17 | 14 | O | 17.72 | 0.47 | O | 76 | 18 | H | ... | ... |
| A6..... | LHS 1044[e] | 3.55330 | −13.18362 | −554 | −708 | 2 | 2 | U | 15.78 | 0.68 | O | 22 | 6 | H | ... | ... |
| A7..... | J0424−4551[f] | 65.99036 | −45.84513 | −100 | −532 | 15 | 1 | U | 16.85 | 0.73 | O | 34 | 8 | H | ... | ... |
| A8..... | LHS 3917[g] | 348.82831 | −2.16120 | 584 | 192 | 3 | 1 | U | 16.48 | 0.50 | O | 41 | 10 | He | ... | ... |
| A9..... | LHS 4041 | 358.57837 | −36.56524 | 26 | −664 | 1 | 2 | U | 15.46 | −0.02 | O | 59 | 14 | H | −27 | 3 |
| A10..... | JL 193 | 7.85905 | −44.63682 | 342 | 28 | 13 | 10 | U | 16.89 | 0.11 | O | 91 | 24 | He | ... | ... |
| A11..... | LP 880-451[h] | 1.78131 | −31.22642 | 336 | −124 | 3 | 6 | U | 16.47 | −0.12 | O | 108 | 26 | He | ... | ... |
| A12..... | LHS 1076[i] | 6.66973 | −55.41222 | −294 | −450 | 5 | 10 | U | 15.16 | 0.23 | O | 34 | 9 | H | ... | ... |
| A13..... | WD 0252−350[j] | 43.65459 | −34.83158 | 44 | −328 | 2 | 3 | U | 15.79 | −0.05 | O | 71 | 17 | H | 86 | 2 |

NOTES.—The last 13 objects are the new cool WD candidates, coming from the OHDHS sample but not listed in the OHDHS paper. Coordinates are given for epoch and equinox J2000.0. Radial velocities are corrected for gravitational redshift and come from this work, except for A9 and A13 (Pauli et al. 2003).

[a] Astrometry source flag: U is for USNO-B1.0, and O is for OHDHS.

[b] Photometry source flag: S is for CCD photometry from this paper, and O is for data calibrated from OHDHS (SuperCOSMOS) magnitudes.

[c] CMR flag: H is for hydrogen CMR (DA WD), He is for helium CMR, H? is for hydrogen CMR used with H$\alpha$ insecure, He? is for helium CMR used, but it could be a non-DA hydrogen WD, and Sp is for special.

[d] As discussed in § 5.3, C. C. Dahn et al. 2004, in preparation, are about to publish the trigonometric parallax of this WD, showing it to be 30 pc distant and bringing down the redshift-corrected radial velocity to 76 km s$^{-1}$ (H. Harris 2003, private communication).

[e] DA-type, $V = 15.89$, $V-I = 0.67$, and $\pi_{\rm trig} = 51.3 \pm 3.8$ mas (Bergeron et al. 2001).

[f] DA9.5 (Scholz et al. 2000).

[g] DZ7.5, Villanova White Dwarf Catalog (on-line), $V = 16.31$, $V-I = 0.49$, and $\pi_{\rm trig} = 37.5 \pm 5.9$ mas (Bergeron et al. 2001).

[h] DB3, Villanova White Dwarf Catalog (on-line).

[i] DA5, $V = 15.14$, Villanova White Dwarf Catalog (on-line).

[j] Name from Pauli et al. 2003.

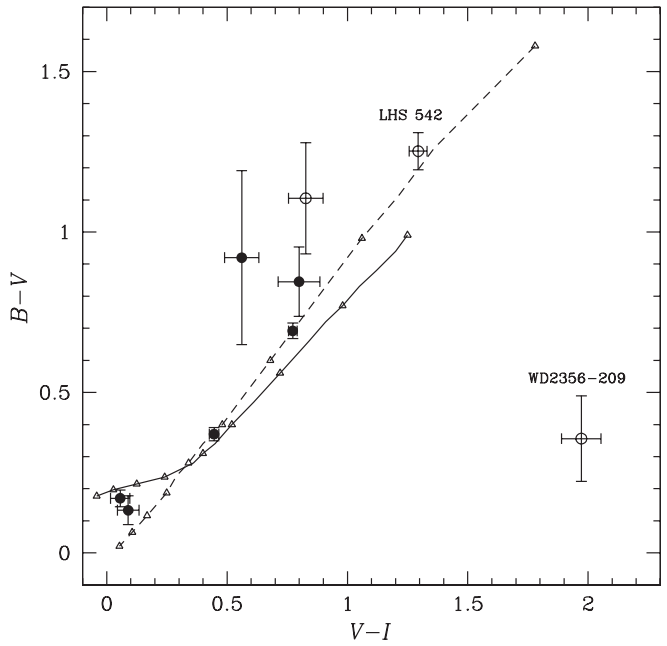


FIG. 2.—$B-V$ vs. $V-I$ color-color diagram of OHDHS cool WDs with CCD photometry. Filled circles show WDs exhibiting the H$\alpha$ line (DA type). The solid and dashed tracks correspond to theoretical colors for $g = 8$ WDs with pure hydrogen and pure helium atmospheres, respectively. The models cover the 4000–12,000 K temperature range, with triangles marking every 1000 K. Labeled objects are discussed in the text.

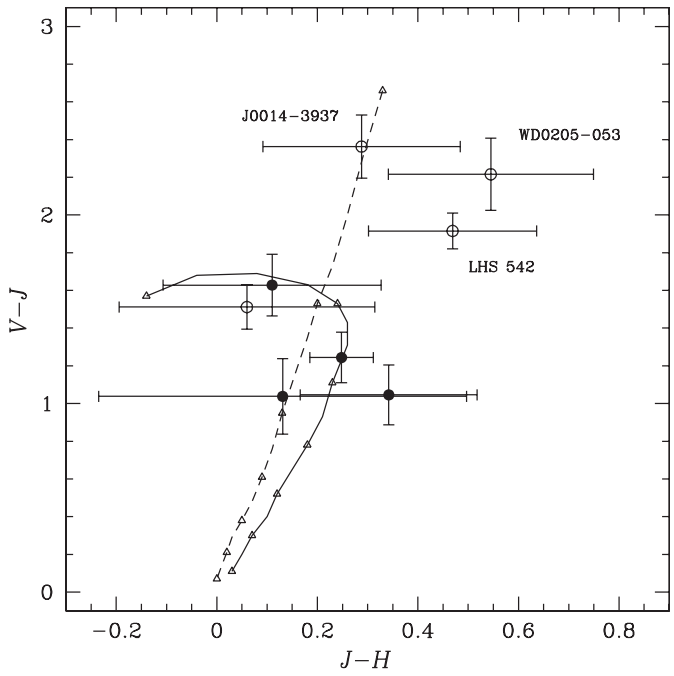


FIG. 3.—$V-J$ vs. $J-H$ color-color diagram of OHDHS cool WDs present in 2MASS. See Fig. 2 for the legend. Tracks terminate at 10,000 K.

the published version, it contains the individual components of the proper-motion error, as does the USNO-B catalog.

USNO-B contains proper motions for 36 OHDHS WDs. The median errors of SuperCOSMOS proper motions are 3.5 times larger than those of USNO-B. We find no systematic differences in the two proper-motion data sets. The reduced $\chi^2$ between the two data sets is 0.8, indicating a good estimate of errors. (SuperCOSMOS proper motions were also recently found by Digby et al. 2003 to agree with proper motions derived by combining SuperCOSMOS and SDSS positions.) There are four cases in which either of the components is discrepant at a more than 2 $\sigma$ level. In all of these cases, the listed error of USNO-B proper motions is rather large, and also larger than the SuperCOSMOS listed error. Visual inspection of Digitized Sky Survey (DSS1 and DSS2) images confirms the SuperCOSMOS value. Again, this is in line with Gould (2003), who found that when USNO-B errors have large values, they are usually underestimated. Thus, except for these four cases, and for one other in which USNO-B error is significantly larger than for SuperCOSMOS, in Table 4 we mostly list USNO-B values, with a flag indicating the source of proper motion.

### 4.3. *Distances*

#### 4.3.1. *Colors and Atmospheric Composition*

In principle, multiband photometry allows a determination of the temperature of a WD and its atmospheric composition. In practice, we are often limited by the range of photometric measurements and their precision. Nevertheless, construction of color-color diagrams can be useful in some cases.

From our CCD photometry we can place nine OHDHS WDs onto a *BVI* diagram (Fig. 2). The solid and dashed tracks correspond to theoretical colors for $g = 8$ WDs with pure hydrogen and pure helium atmospheres, respectively, taken from Bergeron, Saumon, & Wesemael (1995a) and Bergeron, Wesemael, & Beauchamp (1995b). Tracks go from 12,000 K on the blue end to 4000 K. Filled symbols correspond to WDs showing an H$\alpha$ line (therefore being of the DA type). Judging from the position in the diagram, DA WDs are consistent with the hydrogen track, as expected. Of the three non-DA WDs, LHS 542 is clearly not consistent with a hydrogen atmosphere. As shown by Bergeron et al. (2001), a He atmosphere represents a good fit to LHS 542 optical and infrared photometry. More interesting is another non-DA WD, 2356−209, an obvious outlier in the color-color diagram. OHDHS have already shown its spectrum, suggesting that it had "no analogs." Our LRIS spectra confirm this, and so does the photometry; we see excessively blue $B-V$ color for an extremely red $V-I = 1.97$.[8] It has been suggested (I. N. Reid 2003, private communication) that the heavy blanketing in the blue part of the spectrum is due to an extremely broad Na I doublet (which would make this WD a DZ type). Indeed, in our low-resolution spectra we see a well-defined dip around 5893 Å. Thus, the subdued flux in the Na I region is consistent with $V-I$ being boosted and $B-V$ becoming blue. Recently, a similar WD was found with an extremely wide Na I absorption line, SDSS J1330+6435 (Harris et al. 2003). The S/N of the SDSS J1330+6435 spectrum is too low to confirm the presence of other lines characteristic of DZ type WDs. Even in our 45 minute low-resolution exposure, we could not positively identify the Ca II triplet. It is possibly absent because of a very low temperature. Finally, the two hottest WDs in our photometry sample are also in this diagram, and judging from their position in it, they seem to have a temperature of $\sim$11,500 K. Their $R$ magnitudes are also consistent with this temperature.

We also look for the OHDHS WDs in the 2MASS All-Sky Point Source Catalog. Nine are cataloged. Since they are at the limits of 2MASS detection, the infrared photometry is

[8] Note that because the $B_J$ bandpass is actually close to $V$, WD 2356−209 did not stand out in the original OHDHS color-color diagram (their Fig. 4).

relatively crude. Actually, one is not detected in $H$ band, and an additional five lack $K_s$ magnitudes. Of these, we have CCD photometry for only three (one of which is LHS 542, discussed above). Therefore, for the remaining WDs we use a calibration between $V$ and $B_J$ (eq. [4]), whose accuracy is comparable to that of 2MASS magnitudes. We then plot $V-J$ against $J-H$ in Figure 3. Again, we can see that all WDs with H$\alpha$ are compatible with models with pure hydrogen atmospheres (Bergeron et al. 1995a). Three do not seem to be consistent with $H$ colors, of which one is LHS 542. The other two (WD 0205−053 and J0014−3937) are even cooler, with a temperature of $\sim$4200 K.

Therefore, based on optical and infrared color information, we can conclude that four WDs in the sample probably have He atmospheres: LHS 542, WD 2326−272, J0014−3937, and WD 0205−053. In addition, Bergeron (2003), based on OHDHS photometry alone, finds that WD 0125−043 and LHS 1447 are better fit with a He model.

Moreover, there are three additional WDs with $V-I > 1.4$, a red color that hydrogen WDs cannot attain. Finally, there are two WDs with peculiar spectra (the previously mentioned WD 2356−209 and LHS 1402), which are treated separately.

This leaves 11 cool WDs that, based on the above arguments, could have either hydrogen or helium atmospheres. In order to use the appropriate color-magnitude relation (CMR), we would like to classify these remaining WDs as well. Bergeron, Ruiz, & Leggett (1997) have shown that all hydrogen WDs with $T \gtrsim 5000$ K ($V-I \lesssim 1.0$) should exhibit absorption lines. There are four such WDs without H lines, to which we thus assign He atmospheres. We also see that of six WDs likely to have He atmospheres based on color-color diagrams, all but LHS 1447 (a He WD candidate based on the Bergeron et al. 2001 analysis of the original OHDHS photometry) have $V-I \gtrsim 0.8$. Therefore, for the remaining seven WDs (with $1.1 < V-I < 1.3$), we also adopt He composition but allow for the possibility of misclassification. Atmosphere assignments are given in Table 4.

#### 4.3.2. *Color-Magnitude Relations*

Currently, only LHS 542 has a good trigonometric parallax measurement, with an accuracy of 12% (but see § 5.3). Therefore, we have to rely on photometric distances. It is to this end that we have acquired precise $V-I$ CCD photometry. This was accomplished for half of the sample. However, the CCD photometry also allowed the remaining WDs with only photographic photometry to be transformed into standard magnitudes (§ 3.2). Note that the calibrations between the plate and the standard magnitudes that appear in the literature were not measured (or modeled) for WDs (e.g., Bessell 1986; Blair & Gilmore 1982), so their use might introduce systematic offsets. On the other hand, our calibration is direct and so should be free of *systematic* effects and accurate enough that it will not dominate in the final distance error.

Next, we need to decide what CMR to use. Here we have a choice between using an empirically measured relation (from WDs with trigonometric parallaxes) or a model relation.

The most widely used empirical CMR is the one based on the Bergeron et al. (2001) multiband photometry of 152 WDs with measured parallaxes. The sample is assembled from heterogeneous sources and is dominated by disk WDs. A linear weighted fit to these WDs (of both DA and non-DA type) produces a relation in $V-I$:

$$M_V = (2.72 \pm 0.09)(V-I) + (12.39 \pm 0.07). \quad (7)$$

This relation has a reduced $\chi^2 = 27$, indicating that we are sampling a range of WD masses or that some measurements are affected by multiplicity. OHDHS used Bergeron et al. (2001) empirical data to construct their CMR, and then used model spectra with model bandpasses to convert standard magnitudes into plate magnitudes.

In this paper, for deriving the distances, we assume a constant WD mass of 0.6 $M_\odot$ and thus use model cooling curves for hydrogen and helium WDs. Surely, readers can use our photometry and a CMR of their choice to arrive at different distance estimates.

For H atmospheres we use the Bergeron et al. (2001) model CMR for a WD mass of 0.6 $M_\odot$. Cooling tracks for other masses are practically parallel, thus changing only the zero point of the relation:

$$M_V = 3.42(V-I) + 11.7 \quad (V-I < 1.3), \quad (8)$$

which is obviously steeper than the empirical relation given in equation (7).

For helium atmospheres, again using the 0.6 $M_\odot$ cooling curve of Bergeron et al. (2001), the following linear fit is appropriate for the color range of interest:

$$M_V = 2.38(V-I) + 12.7 \quad (V-I > 0.8). \quad (9)$$

The helium relation, on the other hand, is somewhat less steep than the empirical relation, at least for this red-color region. In our cool WD sample, there are two WDs with likely helium atmospheres that are bluer than the above range. For them, we read values of $M_V$ directly from the He cooling curve.

As mentioned in § 4.3.1, for seven WDs we simply assume He composition based on color. If this assumption were not true, what would be the error due to using the wrong CMR? For $V-I \lesssim 0.9$, H and He cooling tracks almost coincide, so there would be almost no difference. For redder WDs, the error due to possible misclassification would be

$$\sigma_{M_V}(\text{class}) = 1.10(V-I-1) + 0.13 \quad (V-I > 0.9). \quad (10)$$

The CMRs given above were constructed for fixed masses of 0.6 $M_\odot$. Various studies agree that this is a typical WD mass. However, the spread of masses seems to be less well known and ranges over as much as a factor of 4 (for a review, see Silvestri et al. 2001). To be conservative, we assume a value close to the higher estimates, $\sigma_M = 0.2\ M_\odot$. This mass range translates into an absolute magnitude uncertainty of

$$\sigma_{M_V}(\text{H}) = 0.44, \quad \sigma_{M_V}(\text{He}) = 0.50, \quad (11)$$

which we use with the above CMRs.

#### 4.3.3. *Peculiar White Dwarfs*

As noted previously, the OHDHS cool WD sample contains two objects with peculiar properties. It would therefore be inappropriate to assign $M_V$ to these objects based on $V-I$ color alone.

LHS 1402 has an extremely blue color of $V-I = -0.372$ (CCD photometry). Taken at face value, this would indicate an extremely hot WD, with a temperature in excess of 100,000 K. Alternatively, this could be a very cool hydrogen WD for which the blue color is the result of collision-induced absorption by $H_2$ molecules (Saumon et al. 1994; Hansen 1998).

In a pure hydrogen model this would indicate a temperature of only $\sim$2000 K and an $M_V$ of 18–19 (Saumon & Jacobson 1999). However, Bergeron & Leggett (2002) have recently analyzed two somewhat redder WDs with similar spectra and have concluded that strong infrared suppression is better explained using a *mixed* H/He model in which He dominates. Thus, using a mixed model with $N(\mathrm{H})/N(\mathrm{He}) = 10^{-5}$ and $g = 8$ for LHS 1402, we obtain $T = 3000$ K and $M_V = 16.4$. Note that LHS 1402 is discussed in Bergeron (2003) as possibly having a pure hydrogen atmosphere and thus being extremely faint and close. However, our LRIS spectra do not show a dip at 0.8 $\mu$m, suggesting that the mixed model is a better explanation. In either case, this could well be the coolest WD known.

Another WD with a peculiar spectral energy distribution, WD 2356−209, has already been discussed in terms of its photometry. One cannot use its very red $V-I = 1.972$ to derive $M_V$ from CMR. It seems likely that its temperature is in the 3500–4500 K range (Bergeron 2003), and thus we conservatively assign $M_V = 16.5 \pm 1.0$ to this object.

#### 4.3.4. *Derived Distances*

Finally, we use the appropriate CMRs to get absolute magnitudes and thus the distance estimates from the $V-I$ color, both for the CCD photometry sample and for the sample with photometry calibrated from plates, using equations (4) and (5). To get a total error in absolute magnitude, we add in quadrature the error in $M_V$ due to the uncertainty in $V-I$ color, the uncertainty due to a possible range of WD masses (eq. [11]), and the uncertainty due to possible misclassification, where appropriate (eq. [10]). The error in $V$ magnitude is mostly negligible and is correlated with the $V-I$ error, so we ignore it in calculating the distance error. The resulting distances and their errors are listed in Table 4.

For LHS 542 we thus obtain a distance of $31 \pm 7$ pc, in agreement with the trigonometric parallax distance of $31.1 \pm 3.6$ pc. Mostly because of allowing for a large scatter in WD masses, our estimate of the typical distance error is 24%. If the spread in masses were actually 2 times smaller (0.1 $M_\odot$), the distance error would also be approximately cut in half. Our main goal, however, was to eliminate possible *systematic* errors that would affect the kinematics and thus the interpretation of results. In the future, the parallaxes should provide a definitive check.

Next, we compare the distances obtained here with those listed in OHDHS. Taken together (but omitting the two peculiar WDs), our new distances are 16% *larger* than those of OHDHS (13% if only WDs with CCD photometry are considered). This difference is not just an overall offset. Namely, for small distances, the two distance estimates agree well, but the difference increases farther out, reaching on average 0.55 mag in distance modulus for the farthest stars (i.e., new estimates are 30% larger). Plotting the difference against $V-I$ shows a very similar trend; new distances are larger for the blue (almost exclusively hydrogen) WDs. This is suggestive of the fact that the difference arises from our use of model CMRs, which for hydrogen WDs (eq. [8]) have a steeper slope than the empirical CMR (eq. [7]), the type used by OHDHS. To test the significance of this effect, we recalculated all distances using the *empirical* CMR (eq. [7]). The trend still exists but is 3 times smaller.

### 4.4. *New Cool White Dwarf Candidates*

The OHDHS cool WD sample of 38 stars was selected based on their high velocities in the $U$-$V$ plane. Does our recalibration of distances make some WDs exceed the velocity cutoff that they previously were not able to reach? To answer this, we look at 60 WDs that were identified by OHDHS but had $U$-$V \leq 94$ km s$^{-1}$. This list was not published in OHDHS but is available on-line, at the URL given in footnote 7. Of 60 WDs, 39 have both $B_J$ and $I_N$ magnitudes available, so we use equations (4) and (5) to get $V$ and $V-I$. For the remaining 21 WDs we obtain $V$ and $V-I$ from $B_J$ and $R_{59F}$, again calibrated using our CCD photometry. We then find provisional distances according to the hydrogen CMR (eq. [8]), for all objects with $V-I < 0.8$, and the helium CMR (eq. [9]), for red objects. Such assignment is conservative, so that even if an incorrect CMR is used, a WD will not be excluded.

In this sample we notice two objects with predicted distances of only 7 pc. We identify one as LHS 69, a known nearby non-DA WD (Bergeron et al. 2001). Its trigonometric parallax gives a distance of $8.1 \pm 0.3$ pc. It has a standard $V = 15.71$ (we predict 15.69). The second is also a known WD with a mixed atmospheric composition (Bergeron et al. 1994), LHS 1126, at a trigonometric distance of $9.9 \pm 1.0$ pc and having $V = 14.50$ (predicted 14.37). Both of these cases provide additional support to our calibration of plate photometry and method for estimating distances not being biased.

In this sample, with new distances, we find an additional 13 WDs, previously falling below the velocity cutoff, to have $U$-$V > 94$ km s$^{-1}$. The predicted $U$-$V$ plane velocities of these new cool WD candidates reach as high as 157 km s$^{-1}$ in the case of LHS 4041. Actually, this WD and one other of the 13 (WD 0252−350) have actually already been proposed, based on all three components of the velocity, as candidate halo members (Pauli et al. 2003). Another six objects are also listed in the literature, of which five are spectroscopically confirmed WDs. The full data for these new candidate halo WDs are given in the last 13 rows of Table 4.[9]

The effect goes in the opposite direction as well; some of the original OHDHS cool WDs no longer have estimated $U$-$V$ plane velocities in excess of 94 km s$^{-1}$. These are discussed in § 5.2.

Table 4 provides all data or measurements (with errors when applicable) that are required for the kinematical analysis. Besides the original 38 OHDHS cool WDs, we list 13 WDs that qualify after the recalibration. For consistency with the original paper, the names of previously unnamed WDs are constructed from OHDHS J2000.0 coordinates.

## 5. DISCUSSION

### 5.1. *Radial Velocities and the U-V Plane Velocities*

OHDHS selected their sample based on the two components of velocity projected onto the sky. The third component, radial velocity, was not available. In order to obtain components of motion in the Galactic coordinate system ($U$, $V$, $W$), they assumed $W = 0$, which produces some arbitrary radial velocity that was then used to calculate $U$ and $V$. Based on these $U$- and $V$-velocities, they selected their cool WD sample. Using the assumption of $W = 0$, rather than $v_{\mathrm{rad}} = 0$, was seen as a potential source of bias (Reid, Sahu, & Hawley 2001; Silvestri, Oswalt, & Hawley 2002). The justification given by OHDHS is

[9] Here we note that H. Harris (2003, private communication) has pointed out that one of the low-velocity objects, WD 0117−044, is actually an almost equal WD binary, separated by 3″, and has measured for component A $V = 18.14 \pm 0.03$, $B-V = 0.90 \pm 0.05$, $V-I = 1.00 \pm 0.03$, and for B, $V = 18.17 \pm 0.03$, $B-V = 0.95 \pm 0.05$, $V-I = 0.96 \pm 0.04$. This would make the distance estimate, and thus the velocity, larger. However, using the USNO-B proper motion, it still falls somewhat short of the 94 km s$^{-1}$ cut.

based on the fact that their sample is mostly in the direction of a Galactic pole, so $U$ and $V$ should not be much affected by the $W$-component.

For our radial velocity sample of OHDHS WDs, we can calculate the actual velocity components $U$, $V$, and $W$ and thus directly test and quantify the validity of the $W = 0$ assumption. In Figure 4 we plot as open squares the original[10] OHDHS positions of 13 WDs with radial velocities and as filled squares their positions when the radial velocities are taken into account. To help match the corresponding points, we put sequential numbers next to them. We see that the changes range from negligible to moderately high (point 12 is LHS 4033 moved by 81 km s$^{-1}$). On average, the points move by 29 km s$^{-1}$. What about the change in $U$-$V$ plane velocity? First, we see that as a result of accounting for radial velocity, two objects that were just outside of the 94 km s$^{-1}$ cut have moved inward. These two cases actually represent the largest changes ($-48$ and $-58$ km s$^{-1}$), while the average change is just $-5$ km s$^{-1}$. On average, each individual $U$-$V$ plane velocity is smaller by 6% (with a scatter of 21%). Thus, it seems that this is a modest effect and that the use of the $W = 0$ assumption in the absence of radial velocities is appropriate for this sample. Note that in this comparison we kept the sky-projected (tangential) velocities the same, i.e., we used the original OHDHS values.

### 5.2. *New Distances and the U-V Plane Velocities*

Newly determined distances will, through modified sky-projected velocities, directly affect the derived values of $U$- and $V$-velocity components. We already saw the result of this in § 4.4, in which the new distances produced 13 new cool WD candidates with potential halo kinematics. In addition, in § 4.3.4 we saw that there is a systematic trend affecting large distances more than the nearby ones. Since on average we expect high $U$-$V$ values to belong to farther objects, we would expect this trend to be reflected in the $U$-$V$ plane. The revised proper motions will also be responsible for some change, albeit a very slight one.

[10] Note that here, and in the entire paper, for LP 651-74 (line 36 in the OHDHS Table 1) we use $B_J - R_{59F} = 0.72$, and thus the OHDHS distance of 39 pc, in accordance with the on-line list.

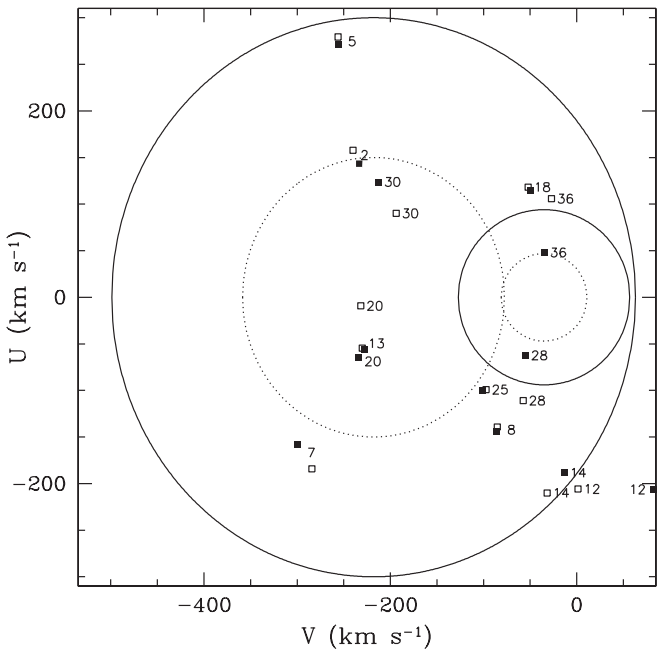


FIG. 4.—Effect of radial velocities on the $U$-$V$ plane kinematics. We plot the original OHDHS positions of our radial velocity sample (*open squares*) and their positions in the $U$-$V$ plane after the radial velocities have been taken into account (*filled squares*). Numbers should help match the corresponding points.

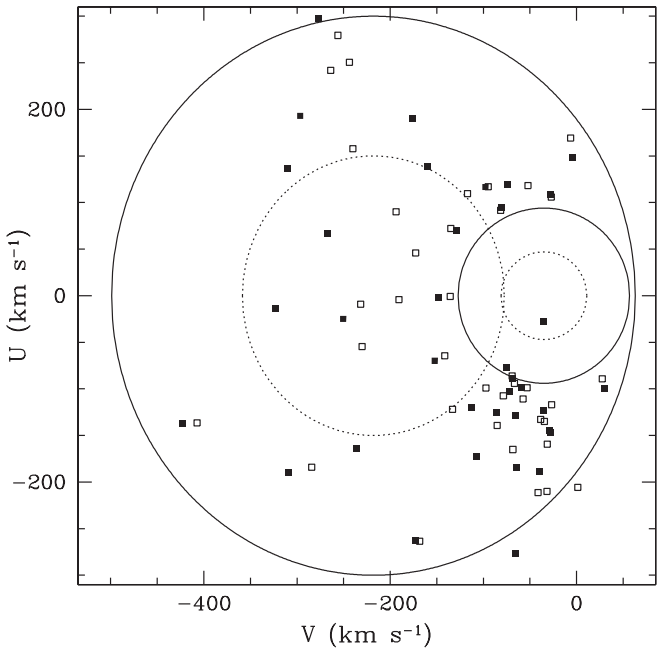


FIG. 5.—Effect of recalibrated distances on the $U$-$V$ plane velocities. The original velocities of 38 OHDHS cool WDs are shown as open squares (corresponding to their Fig. 3), while values obtained with new distances (and proper motions) are shown as filled squares.

In Figure 5 we show the new (*filled squares*) and the original (*open squares*; equivalent to OHDHS Fig. 3) $U$-$V$ plane positions of the 38 OHDHS WDs. In both cases the radial velocities are neglected, i.e., $W = 0$. To avoid clutter, individual points are not labeled, yet we notice that the new $U$-$V$ plane velocities tend to be higher, especially for already high values. The analysis shows that on average, points have moved by 46 km s$^{-1}$, while the $U$-$V$ plane velocity on average has increased by 23 km s$^{-1}$ (with the maximum change being +171 km s$^{-1}$). Each individual $U$-$V$ plane velocity is on average larger by 10% (with a scatter of 30%).

Thus, the net effect of radial velocities and new distance determinations is that the average $U$-$V$ plane velocities are somewhat higher than the original ones.

### 5.3. *Velocity Component Perpendicular to the Galactic Plane*

For our radial velocity subsample of 13 WDs, we can determine the true velocities in the direction perpendicular to the Galactic plane: the $W$-component. We plot the $W$-values in Figure 6 as a function of the $U$-$V$ plane velocity. We have also added two WDs from the newly qualified cool WDs that have radial velocities measured by Pauli et al. (2003; *open circles*). Omitting the two WDs with $U$-$V \leq 94$ km s$^{-1}$, we find the $W$-dispersion of the LRIS sample to be $\sigma_W = 59$ km s$^{-1}$. Only one WD (LHS 4033, $V-I = 0.06$) exceeds 100 km s$^{-1}$, reaching $W = -153$ km s$^{-1}$. Without it, we would have $\sigma_W = 44$ km s$^{-1}$. Actually, C. C. Dahn et al. (2004, in preparation) are about to publish the trigonometric parallax for this WD. It turns out that LHS 4033 is very massive ($M = 1.25\ M_\odot$) and thus some 3 times closer than estimated based on a 0.6 $M_\odot$

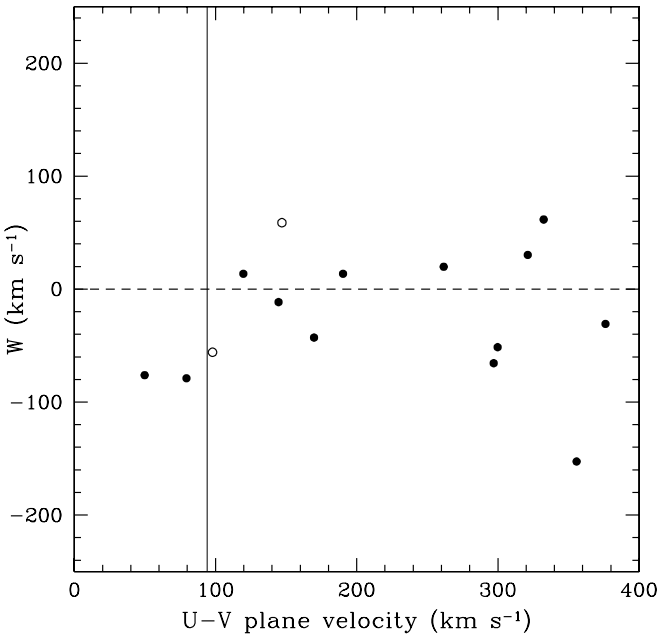


FIG. 6.—Component of motion perpendicular to the Galactic plane. The $W$-velocities of 13 OHDHS WDs with radial velocities measured by us are shown as filled circles. Two open circles come from the "additional" cool WD candidates and were measured by Pauli et al. (2003). The vertical line represents the $U$-$V = 94$ km s$^{-1}$ cut.

CMR. This measurement also affects its surface gravity, producing a much larger gravitational redshift than we assume for our WDs. Altogether, if one were to use this information a posteriori (which can be strongly argued against), one would get $\sigma_W = 45$ km s$^{-1}$. At any rate, these values are between the values usually derived for thick-disk and spheroid (halo) populations, 35 and 94 km s$^{-1}$, respectively (Chiba & Beers 2000). That the radial velocity sample probes mostly what appears to be a lower velocity (and younger?) population was already indicated in § 4.1.3. Indeed, all but three of the radial velocity WDs are proper motion–limited. While one can formally calculate $\sigma_U$ and $\sigma_V$, they are meaningless because of the $U$-$V$ selection that was applied to derive the sample in the first place. We defer a more thorough analysis of the kinematics and population to a forthcoming paper.

### 5.4. *Space Density of White Dwarfs*

The derived space density, and thus the mass density, of the OHDHS cool WDs was their key result, and the one that stirred most controversy, since it is considerably higher than the expected stellar (as opposed to dark matter) halo WD density. Using OHDHS original data for 38 cool WDs and applying the same $1/\mathcal{V}_{\max}$ technique, with a limiting magnitude of $R_{59F}^{\lim} = 19.8$, one derives $n = 1.4 \times 10^{-4}$ pc$^{-3}$ (close to the value given by OHDHS of $1.8 \times 10^{-4}$ pc$^{-3}$). Using a typical WD mass of 0.6 $M_\odot$, this corresponds to $\rho = 8.3 \times 10^{-5}$ $M_\odot$ pc$^{-3}$, or some 6 times higher than the canonical value of stellar-halo WD mass density of $\rho_c = 1.3 \times 10^{-5}$ $M_\odot$ pc$^{-3}$ (Gould, Flynn, & Bahcall 1998). (Note that this often-quoted *canonical* value is somewhat of an educated guess and not a real measurement; A. Gould 2003, private communication).

What estimate of density would we get with our updated data? In our analysis we include all cool WD candidates from Table 4, using the radial velocity data where available. For completeness, we append this list to the remaining low-velocity WDs identified by OHDHS ($U$-$V \leq 94$ km s$^{-1}$). For them, we use listed SuperCOSMOS proper motions and do not check for the availability of radial velocities in the literature. Looking at the entire WD sample of 98 objects will allow us to characterize the density not just for a subsample with a fixed $U$-$V$ cut but also as a function of the $U$-$V$ cutoff velocity.

Of 47 WDs with $U$-$V > 94$ km s$^{-1}$, only 12 are magnitude-limited. All others, including all 51 WDs with $U$-$V \leq 94$ km s$^{-1}$, are proper motion–limited; that is, the maximum distance at which they could be detected is determined by the proper-motion lower limit of the survey (330 mas yr$^{-1}$). For the magnitude limit we use $R_{59F}^{\lim} = 19.8$, transformed for each object into a corresponding $V^{\lim}$ using equation (2).

If we restrict ourselves to the original $U$-$V$ cut of 94 km s$^{-1}$, the 47 WDs that make this cut yield

$$n_{94} = 1.72 \times 10^{-4} \text{ pc}^{-3}, \tag{12}$$

which is similar to or slightly higher than the original estimate based on 38 WDs and $R_{59F}^{\lim} = 19.8$. For this sample we have $\langle \mathcal{V}/\mathcal{V}_{\max} \rangle = 0.51$, suggesting that $R_{59F}^{\lim}$ has an appropriate value.

How sensitive is this estimate to the choice of $U$-$V$ cutoff velocity? In Figure 7 we plot the cumulative number density starting from the *highest* $U$-$V$ values (*dotted line*). However, since at higher $U$-$V$ values we limit ourselves to a yet smaller portion of the $U$-$V$ plane, we need to correct it. We do it by finding (at each $U$-$V$) a fraction of objects with Chiba & Beers (2000) halo kinematics that get excluded by different $U$-$V$ cuts. (The correction factor is normalized to 1 for $U$-$V =$ 94 km s$^{-1}$, in order to make the results directly comparable to OHDHS, who did not perform this correction. In any case, the actual correction at this velocity is very small.)

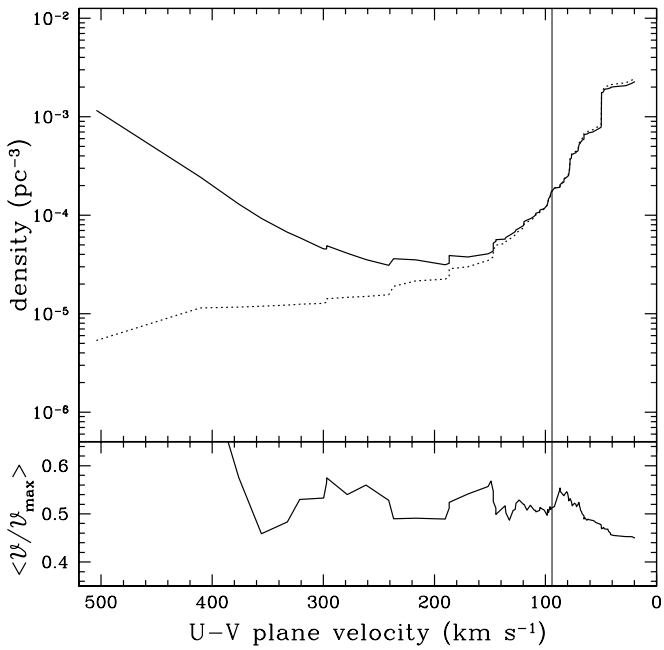


FIG. 7.—Number density of OHDHS WDs as a function of the $U$-$V$ velocity cut. *Top*: Corrected (*solid line*) and uncorrected (*dotted line*) cumulative density of all 98 WDs observed by OHDHS (summing from the high-velocity end). The corrected line takes into account that at high $U$-$V$ values we sample a smaller part of the $U$-$V$ plane. The vertical line represents the $U$-$V = 94$ km s$^{-1}$ cut. *Bottom*: Average $\langle \mathcal{V}/\mathcal{V}_{\max} \rangle$ as we move toward the lower $U$-$V$-velocities. Note that beyond $\sim$300 km s$^{-1}$ we have only a couple of objects.

The corrected densities are shown with a solid line. Figure 7 (*bottom*) monitors $\langle \mathcal{V}/\mathcal{V}_{\max} \rangle$ at each point and appears consistent with 0.5 for the entire range of interest. The vertical line denotes the 94 km s$^{-1}$ limit. Inward of this limit we have a rise of density due to nonhalo populations. Actually, we see that this rise begins inward of $U$-$V \sim 150$ km s$^{-1}$. Note that in the *corrected* plot, the density of objects with halo kinematics should be independent of the $U$-$V$ cut. The corrected density at $U$-$V = 150$ km s$^{-1}$ is

$$n_{150} = 0.42 \times 10^{-4} \text{ pc}^{-3}, \quad (13)$$

corresponding to $1.9\rho_c$. The minimum value of the attained density is

$$n_{\min} = 0.31 \times 10^{-4} \text{ pc}^{-3} \quad (14)$$

at $U$-$V \sim 190$ km s$^{-1}$. This minimum value corresponds to $1.4\rho_c$ within the uncertainty of the stellar-halo WD density.[11] Beyond $U$-$V \sim 250$ km s$^{-1}$, the density estimate rises again. It exceeds $n_{94}$ when $U$-$V > 400$ km s$^{-1}$. However, in this range, the density is based on just the two or three highest velocity objects with huge correction factors.

[11] Note that the C. C. Dahn et al. (2004, in preparation) result on LHS 4033 would only slightly affect $n_{94}$ (increasing it by 5%) and would leave $n_{150}$ and $n_{\min}$ unchanged.

## 6. CONCLUSIONS

We obtain precise radial velocities for the majority of OHDHS WDs with H$\alpha$ lines. This makes it possible to measure more precisely the $U$- and $V$-components of the velocity and also allows the $W$-component to be derived. We show that the radial velocities do not affect significantly the way in which OHDHS selected their cool WD candidates. Our $W$-velocity dispersion lies between the typical thick-disk and halo values, an indication of a mixed sample. In addition, our new CCD photometry, and the recalibration of OHDHS SuperCOSMOS plate photometry, allows for more robust distance estimates.

Finally, with the new data set and applying the same methods of analysis as in OHDHS, we confirm the densities of cool WDs that they derived. However, many times lower densities (consistent with the stellar halo) are found if one adopts higher $U$-$V$ cutoff velocities. This new set of data facilitates a more sophisticated analysis, which we plan to present in a forthcoming paper.

We thank Didier Saumon for valuable discussions and the referee Hugh Harris for sharing some unpublished measurements. We are indebted to Nigel Hambly and Andrew Digby for their work in constructing the SuperCOSMOS sample. This publication makes use of the VizieR and SIMBAD Catalogue Services of CDS in Strasbourg, France, and data products from 2MASS, which is a joint project of the University of Massachusetts and IPAC/Caltech, funded by NASA and the National Science Foundation.

## REFERENCES

Afonso, C., et al. 2003, A&A, 400, 951
Alcock, C., et al. 2000, ApJ, 542, 281
Bergeron, P. 2003, ApJ, 586, 201
Bergeron, P., & Leggett, S. K. 2002, ApJ, 580, 1070
Bergeron, P., Leggett, S. K., & Ruiz, M. T. 2001, ApJS, 133, 413
Bergeron, P., Ruiz, M., Leggett, S. K., Saumon, D., & Wesemael, F. 1994, ApJ, 423, 456
Bergeron, P., Ruiz, M. T., & Leggett, S. K. 1997, ApJS, 108, 339
Bergeron, P., Saumon, D., & Wesemael, F. 1995a, ApJ, 443, 764
Bergeron, P., Wesemael, F., & Beauchamp, A. 1995b, PASP, 107, 1047
Bessell, M. S. 1986, PASP, 98, 1303
Blair, M., & Gilmore, G. 1982, PASP, 94, 742
Chiba, M., & Beers, T. C. 2000, AJ, 119, 2843
Digby, A. P., Hambly, N. C., Cooke, J. A., Reid, I. N., & Cannon, R. D. 2003, MNRAS, 344, 583
Eggen, O. J., & Sandage, A. 1967, ApJ, 148, 911
Freese, K., Fields, B., & Graff, D. 2000, in The First Stars, Proc. MPA/ESO Workshop, ed. A. Weiss, T. G. Abel, & V. Hill (New York: Springer), 18
Garnavich, P. M., et al. 1998, ApJ, 493, L53
Gould, A. 2003, AJ, 126, 472
Gould, A., Flynn, C., & Bahcall, J. N. 1998, ApJ, 503, 798
Hambly, N. C., Davenhall, A. C., Irwin, M. J., & MacGillivray, H. T. 2001a, MNRAS, 326, 1315
Hambly, N. C., Irwin, M. J., & MacGillivray, H. T. 2001b, MNRAS, 326, 1295
Hambly, N. C., et al. 2001c, MNRAS, 326, 1279
Hansen, B. M. S. 1998, Nature, 394, 860
Hansen, B. M. S., & Liebert, J., 2003, ARA&A, 41, 465
Harris, H. C., et al. 2003, AJ, 126, 1023
Lasserre, T., et al. 2000, A&A, 355, L39
Liebert, J., Dahn, C. C., & Monet, D. G. 1988, ApJ, 332, 891
Monet, D. G., et al. 2003, AJ, 125, 984
Oke, J. B., et al. 1995, PASP, 107, 375
Oppenheimer, B. R., Hambly, N. C., Digby, A. P., Hodgkin, S. T., & Saumon, D. 2001, Science, 292, 698 (OHDHS)
Paczyński, B. 1986, ApJ, 304, 1
Pauli, E.-M., Napiwotzki, R., Altmann, M., Heber, U., Odenkirchen, M., & Kerber, F. 2003, A&A, 400, 877
Reid, I. N. 1996, AJ, 111, 2000
Reid, I. N., Sahu, K. C., & Hawley, S. L. 2001, ApJ, 559, 942
Riess, A. G., et al. 1998, AJ, 116, 1009
Sahu, K. C. 1994, Nature, 370, 275
Saumon, D., Bergeron, P., Lunine, J. I., Hubbard, W. B., & Burrows, A. 1994, ApJ, 424, 333
Saumon, D., & Jacobson, S. B. 1999, ApJ, 511, L107
Scholz, R.-D., Irwin, M., Ibata, R., Jahreiss, H., & Malkov, O. Y. 2000, A&A, 353, 958
Silvestri, N. M., Oswalt, T. D., & Hawley, S. L. 2002, AJ, 124, 1118
Silvestri, N. M., Oswalt, T. D., Wood, M. A., Smith, J. A., Reid, I. N., & Sion, E. M. 2001, AJ, 121, 503